Biomacromolecules

pubs.acs.org/Biomac

Article

Topochemical Design of Cellulose-Based Carriers for Immobilization of Endoxylanase

Pieter De Wever, Charlotte De Schepper, Claude Poleunis, Arnaud Delcorte, Christophe M. Courtin, and Pedro Fardim*

Cite This: *Biomacromolecules* 2023, 24, 132−140

Read Online

ACCESS | Metrics & More | Article Recommendations

ABSTRACT: Xylooligosaccharides (XOSs) gained much attention for their use in food and animal feed, attributed to their prebiotic function. These short-chained carbohydrates can be enzymatically produced from xylan, one of the most prevalent forms of hemicellulose. In this work, endo-1,4-β-xylanase from *Thermotoga maritima* was immobilized on cellulose-based beads with the goal of producing xylooligosaccharides with degrees of polymerization (DPs) in the range of 4−6 monomeric units. More specifically, the impact of different spacer arms, tethers connecting the enzyme with the particle, on the expressed enzymatic activity and oligosaccharide yield was investigated. After surface functionalization of the cellulose beads, the presence of amines was confirmed with time of flight secondary ion mass spectrometry (TOF-SIMS), and the influence of different spacer arms on xylanase activity was established. Furthermore, XOSs (DPs 2−6) with up to 58.27 mg/g xylan were obtained, which were greatly enriched in longer oligosaccharides. Approximately 80% of these XOSs displayed DPs between 4 and 6. These findings highlight the importance of topochemical engineering of carriers to influence enzyme activity, and the work puts forward an enzymatic system focusing on the production of longer xylooligosaccharides.

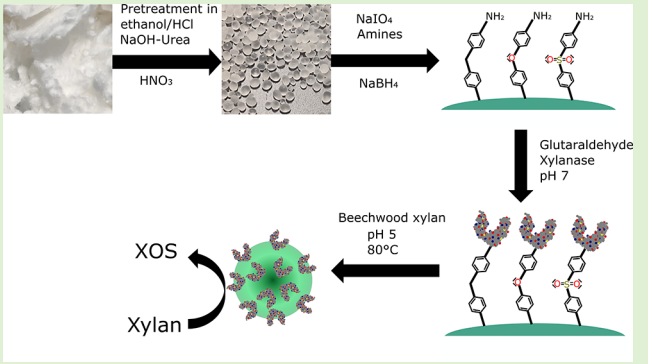

INTRODUCTION

The human gastrointestinal tract is colonized by a microbiome composed of microorganisms rich in diversity, which directly and indirectly influences the host's health. Their impact could be therapeutic or prophylactic in nature.[1] Disruption of a healthy gastrointestinal microbiota poses an increasing risk of suffering from irritable bowel syndrome, type 2 diabetes mellitus, and cardiovascular diseases.[2−5] Strong evidence of a connection exists between certain psychiatric illnesses and gastrointestinal problems.[6] The growth of favorable gastrointestinal microbiota can be promoted by the intake of probiotics, which are beneficial microorganisms, and prebiotics, which are substrates stimulating proliferation of benign bacteria and fungi.[7] Among prebiotics, there exist nondigestible carbohydrates that are instead fermented by the gut microbiota creating short-chained fatty acids in the process. These fatty acids are further digested by the host.[3,8−10] In carbohydrate prebiotics, the degree of polymerization is limited to 60 units depending on the carbohydrate source.[11]

Xylooligosaccharides are short-chained carbohydrates existing out of xylose units connected by β-1,4-glycosidic bonds and may contain substituent groups such as arabinose, acetic acid, and 4-*O*-methylglucoronic acid. The industrial fabrication of xylooligosaccharides from xylan relies on either an acid or enzymatic hydrolysis process. The downside to the former method is the formation of side products such as furfural, which makes the enzymatic method in an industrial setting more appealing.[12,13] The enzymatic xylan hydrolysis also has its challenges: the enzymes have a limited half-life time, the stability is both pH- and temperature-dependent, and the protein recovery is challenging.[13] Immobilizing xylanase on a solid carrier has the advantage of increasing enzyme stability and moreover offers the opportunity to work in packed bed setups.[14−16] The big appeal regarding the use of xylanase for XOSs production is related to their specificity towards distinct xylan sources and their product selectivity. This means that the enzyme activity and the obtained products, which are recovered after xylan hydrolysis, are closely connected to the selection of a specific xylanase, as well as the chosen xylan source.[17−19]

Received: August 11, 2022
Revised: December 2, 2022
Published: December 21, 2022

Downloaded via UNIV CATHOLIQUE DE LOUVAIN on June 1, 2023 at 14:55:21 (UTC).
See https://pubs.acs.org/sharingguidelines for options on how to legitimately share published articles.

ACS Publications

© 2022 American Chemical Society

https://doi.org/10.1021/acs.biomac.2c00998
Biomacromolecules 2023, 24, 132−140

The covalent binding of xylanase has been widely demonstrated on maleic anhydride-,[20] glyoxyl-,[14,21,22] glutaraldehyde-,[23−25] cyanobromide-,[21] and cyanuric chloride[26]-activated supports. This includes more advanced immobilization approaches such as conjugation of customized chimeric[27] enzymes and coating immobilized xylanase with polyethyleneimine.[28] Most conjugation strategies generally involve simple activation of a carrier surface, yet this lacks a surface engineering approach to exploit the full potential of the conjugated protein.

It is generally agreed that a complex interaction exists between the carrier and the protein, which impacts enzyme stability, activity, and selectivity.[16] A well-documented case comprises lipase immobilization on hydrophobic interfaces, resulting in hyperactivation of the particular enzyme.[29,30] Despite great interest in designing immobilized enzyme systems, the topochemical design of carrier interfaces is often overlooked. Topochemical carrier design takes the structure and chemistry of spacer arms into account. As such, Abaházi and co-workers demonstrated the influence of different bisepoxide spacer arms on the activity of *Candida antarctica* Lipase B. Using cyclohexanedimethanol diglycidyl ether as a tether gave rise to an activity of 47.39 μmol min^{-1} g^{-1}, while a polyethyleneglycol diglycidyl ether tether resulted in an activity of just 6.3 μmol min^{-1} g^{-1}.[31] Tiller and co-workers noted that glucose oxidase immobilized with 1,4-bifunctional aromatic cross-linkers displayed higher activity than glucose oxidase immobilized using 1,3-bifunctional aromatic cross-linkers.[32] The spacer arms could also display a buffering effect. Yazgan and co-workers immobilized α-amylase on amino acid-functionalized chitosan and reported that the relation between enzyme stability and changes in pH changed drastically.[33] These studies underline the importance of spacer arms in immobilized enzyme systems.

Cellulose is an abundant biodegradable polymer that can be selectively modified and shaped into porous hydrogel beads.[34] Cellulose hydrogels are fabricated in a two-step approach: dissolution and coagulation steps. The dissolution and coagulation of cellulose has been demonstrated with solvent systems such as aqueous hydroxide solutions[35] and ionic liquids.[36,37] Amino-functionalized cellulose beads are of great interest for immobilizing enzymes. The fabrication of 6-deoxy amino cellulose can be achieved through an intermediate tosylation reaction followed by nucleophilic substitution with a diamine.[38] Conjugation of glucose oxidase, horseradish peroxidase, and lactate oxidase with different cross-linkers has been demonstrated with these cellulose derivatives.[32,39,40] A second method to fabricate amino cellulose starts by subjecting cellulose to periodate oxidation. Periodate oxidation cleaves the C2−C3 bond in the anhydrous glucose unit, creating aldehydes in the process. This functionality can be exploited to graft diamines on the oxidized cellulose.[41−45]

While in general covalent-bound xylanase strongly favors the production of low-DP oligosaccharides, mainly xylobiose and xylotriose, here the target is the synthesis of short-chained sugars with DPs spanning from 4 to 6 xylose units. These compounds also exhibit documented prebiotic function like their lower-molecular-weight counterparts.[12,46,47] On this note, low-DP arabinoxylooligosaccharides supported the production of SCFA's and bifidobacterial levels when supplemented to rat diets, while higher-DP oligosaccharides more effectively suppressed protein fermentation.[48] Moniz and co-workers showed that XOSs from corn straw increased the growth of *Bifidobacterium* and *Bacteroides* populations. The use of specific XOS fractions, DPs ranging either from 9 to 20 or from 4 to 6, greatly impacted the formation of the short-chain fatty acids. The high-DP fraction reached the maximum SCFA concentration after 24 h, greatly exceeding the amount of SCFA produced using low-DP XOSs as a substrate. However, after 24 h, the obtained SCFA, using the 4−6 fraction as a feedstock, rapidly grew toward a similar organic acid concentration.[49] Besides probiotic growth and SCFA production, the degree of polymerization may impact antioxidant activity substantially as demonstrated by the work of Valls and co-workers. Longer XOSs obtained after beechwood xylan hydrolysis, using GH10 xylanase from *Paenibacillus barcinonensis*, provided greater antioxidant activity. In addition, eucalyptus autohydrolysates before a xylanase treatment likewise displayed greater levels of antioxidant activity.[47]

In this work, cellulose beads were modified with three highly similar spacer arms, with minor differences in their structures, to investigate their impact on the expressed enzyme activity and XOS yield. Highly porous carriers favor the production of xylooligosaccharides with low degrees of polymerization (DPs 2−3).[50−52] Therefore, dense functionalized cellulose beads were selected for xylanase conjugation. This is achieved following a topochemical engineering approach in which first dense, air-dried cellulose beads were fabricated. After periodate oxidation, the different spacer arms were grafted on the dialdehyde-activated surface. The composition of the activated surface layer was studied with TOF-SIMS. In the final step, the endo-1,4-β-xylanase from *Thermotoga maritima* was immobilized on the diamine beads in a one-pot reaction with glutaraldehyde.

MATERIALS AND METHODS

4,4′-Methylenedianiline (>98%), 4,4′-oxydianiline (>98%), and 4,4′-sulfonyldianiline (>98%) were ordered from TCI chemicals. Beads functionalized with diamines are hereafter referred to as C-, O-, and S-diamine beads. Beechwood xylan and endo-1,4-β-xylanase from *T. maritima* (100 U/mg), rhamnose, arabinose, xylose, and xylooligosaccharides (DPs 2−6) were purchased from Megazyme. Dissolving pulp from birchwood as a cellulose source was kindly donated by Stora Enso, Finland. Ethanol (>99%), hydrochloric acid (37%), sodium hydroxide (98.5%), nitric acid (69%), sodium periodate ≥99%, glutaraldehyde 25% and sodium tetrahydroborate ≥98% were purchased from VWR. *N*,*N*-Dimethylacetamide (DMAc) (99%) and sodium sulfite (98%) were obtained from Alfa Aesar. Ethylene glycol (technical grade), hydroxylamine hydrochloride (99%), and monopotassium phosphate (>99%) were obtained from Acros Organics. Sodium acetate trihydrate (>99%) and potassium sodium tartrate tetrahydrate (99%) were bought from Sigma Aldrich. Acetic acid was purchased from Fisher, 3,5-dinitrosalicylic acid (99%) from UCB, and phenol (75%) from Applichem.

Fabrication of Cellulose Xerogel Beads. Cellulose beads were fabricated according to the procedure described by Trygg and co-workers.[35] In brief, 16 g of dissolving birchwood pulp was initially treated in a mixture of 400 mL of 92.5% ethanol and 16 mL of 37% hydrochloric acid at 75 °C for 2 h to later facilitate its dissolution in a NaOH−urea solution. The pulp was extensively washed with water and dried. Then, 5.00 g of pretreated pulp was vigorously mixed with 100 g of a 7−12−81% NaOH−urea−water mixture and chilled at −13 °C until completely dissolved. Cellulose beads were obtained after dropping this solution in 400 mL of 2 M nitric acid at room temperature. After 1 h, the swollen beads were washed with water to remove excess nitric acid until a pH of 7 was reached and consequently air-dried. This air-drying caused shrinking and hornification, resulting in the formation of dense, compact xerogel cellulose beads.[34]

https://doi.org/10.1021/acs.biomac.2c00998
Biomacromolecules 2023, 24, 132−140

Functionalization of Beads. Cellulose beads were initially activated through sodium periodate oxidation based on an earlier procedure with some adaptations.[53] To 500 mL of water, 8.12 g of sodium periodate was added, and the flasks were wrapped in an aluminum foil to minimize light exposure to the periodate. Then, 5.00 g of dry cellulose beads were added and allowed to react for 2, 4, and 8 h at room temperature. Oxidized beads were added to ethylene glycol to deactivate the remaining periodate and subsequently extensively washed with water.

Initially, 0.125 mol of the respective diamines, in large excess compared to the oxidized particles, were dissolved in 250 mL of DMAc. Next, the oxidized beads were added and allowed to react for 2 h at room temperature. The formed imine bond was reduced with sodium tetrahydroborate. Amino-activated beads were washed extensively first with DMAc and water afterward. Cellulose beads decorated with 4,4′-methylenedianiline, 4,4′-oxydianiline, and 4,4′-sulfonyldianiline were hereafter, respectively, referred to as C-, O-, and S-diamine beads and are shown in Figure 1.

Figure 1. Dry amine beads were obtained after reacting oxidized cellulose beads with distinct diamines. From left to right, 4,4′-methylenedianiline, 4,4′-oxydianiline, and 4,4′-sulfonyldianiline functionalized beads.

Specific Surface Area. Nitrogen sorption was performed on the amine-activated beads (after an initial 4 h oxidation) using a Mesopore 222 apparatus (3P instruments, Odelzhausen, Germany).

Aldehyde Content. The determination of the aldehyde content is based on the protocol described by Dang and co-workers with minor modifications.[54] Hydroxylamine hydrochloride (20 mL, 0.05 g/mL) was added to 20 mL of distilled water. The pH of the system was adjusted to 4.5 using 0.1 mol/L NaOH. Then, 1.0 g of dry oxidized beads were added to the solution. In a heated shaking water bath, the reaction between the aldehyde and hydroxylamine hydrochloride proceeded at 40 °C for 4 h, liberating HCl in the process. The HCl concentration was determined by titration with 0.1 mol/L NaOH. Blank experiments were executed with unmodified beads. With the titrated volume obtained, the aldehyde content per anhydrous glucose unit (AGU) is calculated as follows:

$$n(\mathrm{CHO}) = 2\frac{c(V_s - V_b)}{m_{beads}} \times \frac{162}{\mathrm{AGU}} \quad (1)$$

where c is the concentration of NaOH, V_s and V_b are the used volumes of the NaOH solution for the oxidized and unmodified beads, respectively, and m_{beads} is the mass of the beads added. The number 162 represents the molar mass of one AGU.

Enzyme Immobilization and Activity Assay. In total, 50 μL of the commercial enzyme stock solution was first diluted in 50 mL of phosphate buffer (pH 7). Then, 0.2 g of diamine beads, 5 mL of the enzyme solution, and 500 μL of 5% glutaraldehyde (GA) were mixed and stirred for 2 h to activate the beads. The beads were repeatedly washed with an acetate buffer (pH 5). Next, the beads were resuspended in 5 mL of a 1% xylan solution with pH 5. The hydrolysis reaction was performed at 80 °C for 10 min. Enzyme activity was determined by monitoring the amount of reducing sugar released through the dinitrosalicylic acid (DNS) assay.[55] The immobilization yield (IY) and activity yield (AY) are defined according to Rajagopalan and co-workers as follows:[51]

$$\mathrm{IY}\ (\%) = \frac{A - B}{A} \times 100\% \quad (2)$$

$$\mathrm{AY}\ (\%) = \frac{C}{A} \times 100\% \quad (3)$$

where A, B, and C represent the activity of the total amount of supplied enzymes, the activity of the supernatant after immobilization, and the activity of the immobilized enzyme, respectively. The production of short-chained xylooligosaccharides was essayed using the diamine particles that were initially oxidized for 4 h. The XOS composition was evaluated with high-performance anion exchange chromatography with integrated pulsed amperometric detection (HPAEC-IPAD) after the enzymatic hydrolysis for 24 h at 80 °C. Rhamnose was added to the XOS mixtures as an internal standard. The calibration was performed with standard solutions of arabinose, xylose (X_1), xylobiose (X_2), xylotriose (X_3), xylotetraose (X_4), xylopentaose (X_5), and xylohexaose (X_6). The XOS yield was calculated after determination of the stoichiometric factors:[52]

$$\mathrm{yield}_{XOS} = (0.936 \times C_2 + 0.956 \times C_3 + 0.967 \times C_4 + 0.973 \times C_5 + 0.977 \times C_6)/(C_{xylan}) \quad (4)$$

where C_n is the concentration of the respective oligosaccharide and C_{xylan} is the initial xylan concentration.

The determination of the aldehyde content, nitrogen sorption, and xylanase immobilization as well as the measurements regarding the enzyme activity was performed in triplicate.

TOF-SIMS Analysis. Samples were chemically characterized using a TOF.SIMS 5 instrument (IONTOF GmbH, Münster, Germany) with a pulsed Bi_5^+ metal ion source, which generated the primary beam using an acceleration voltage of 30 kV. An AC target current of 0.08 pA with a bunched pulse width lower than 1 ns was used. Both positive and negative secondary ion species were collected and analyzed. A raster containing 128 × 128 data points, measured over an area of 250 × 250 μm^2, was used to collect the spectra from the amino cellulose surface. The total primary ion beam dose for each analyzed area was always kept below 5 10^{10} ions cm^{-2}, ensuring static conditions. In both positive and negative spectra acquisition, a lateral resolution of ~3 μm and a mass resolution $m/\Delta m$ of > 4000 at 29 m/z were maintained. Charge compensation was done by an interlaced electron flood gun (E_k = 20 eV). Data analysis was carried out using the software supplied by the instrument manufacturer, SurfaceLab (version 6.8).

RESULTS AND DISCUSSION

Highly swollen porous beads were obtained after dropping the cellulose solution in diluted nitric acid. The obtained cellulose hydrogel spheres were washed with water until the pH remained stable at 7. Air-drying causes the particles to contract and pores to collapse, caused by an irreversible process defined as hornification.[56] The compact cellulose xerogel beads were activated by exploiting highly selective surface oxidation with sodium periodate. To determine the contribution of grafting density on enzymatic activity, the beads were oxidized for different durations. For 2, 4, and 8 h oxidation times, the cellulose beads carry aldehyde contents of, respectively, 0.12 ± 0.01, 0.35 ± 0.08, and 0.72 ± 0.05 aldehydes/anhydrous glucose unit (CHO/AGU). By applying brief oxidation times, the shell of the beads is highly functionalized and it leaves sodium periodate less time to permeate deeply inside the dense cellulose beads. High degrees of periodate oxidation are associated with reduced crystallinity, particularly for cellulose II, which would weaken the stability of the beads in water. Dialdehyde cellulose, with a high degree of substitution, is even claimed to be water-soluble.[57]

Dang and co-workers obtained an aldehyde group content of 0.75 (CHO)/AGU after 5 h oxidation at 30 °C but proved that this could be increased using pretreatments prior to the oxidation or by exploiting electrochemically assisted periodate

https://doi.org/10.1021/acs.biomac.2c00998
Biomacromolecules 2023, 24, 132−140

oxidization.[54] Sirviö and co-workers used 3 h oxidation at 55 °C to obtain cellulose with aldehyde contents of 0.54 (CHO)/AGU and 0.64 (CHO)/AGU.[41] Both these values are considerably higher than the values presented after the 4 h oxidation protocol here, yet lower than the aldehyde contents for beads oxidized for a duration of 8 h.

The periodate oxidation creates the necessary platform to produce amino cellulose beads. In earlier work, Lindh and co-workers demonstrated that amine cross-linked beads could be fabricated from periodate oxidized nanocellulose.[42] Others have decorated dialdehyde cellulose with ethylenediamine,[43] guanidine,[41] and monoamines.[44,45] To ensure that just one end of the diamine was attached to the bead interface, the activation of the beads was performed in a large excess of 4,4′-diaminodiphenylmethane, 4,4-oxydianiline, and 4,4′-sulfonyldianiline. By grafting different diamine spacer arms on the aldehyde-activated bead surface, the objective of this work is to study the effect of the spacer arm on enzyme activity and selectivity. The amines differ in their center moiety connecting the two aromatic rings, as illustrated in Figure 2. This

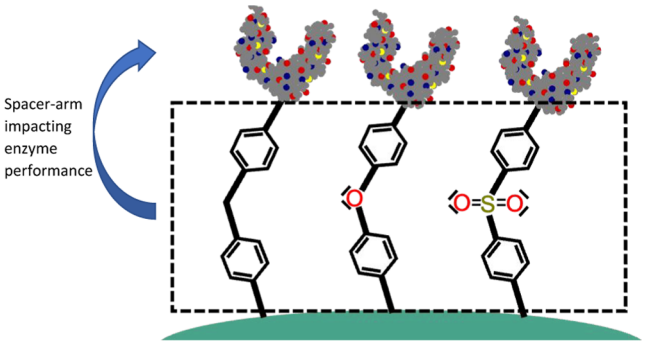

Figure 2. 4,4′-Methylenedianiline (C-) tether on the left, the 4,4′-oxydianiline (O-) tether in the center, and the 4,4′-sulfonyldianiline (S-) tether on the right are grafted on the surface of cellulose beads. The tethers differ in chemical composition between the benzyl groups, thereby exerting differences in dipole moment, creating an altered microenvironment. This altered environment in turn affects enzymatic activity.

functionality generates differences in the diamine's dipole moment, creating an altered microenvironment for enzymes despite the minor differences in the spacer arm structure.

Nitrogen sorption indicated that diamine beads were nonporous, with BET areas <1 m^2/g. The composition of the outermost layer from the dense functionalized beads was analyzed with TOF-SIMS. Samples were examined using the positive and negative ion spectra. Characteristic fragments of the diamine beads are listed in Table 1. For all samples, the positive secondary ions in the TOF-SIMS spectra register the characteristic carbohydrate peaks at m/z 127 and 145 ($C_6H_7O_3^+$ and $C_6H_9O_4^+$, respectively) from the cellulose hexose monomer, while ions $C_5H_7O_3^+$ and $C_5H_9O_4^+$ (m/z 115 and 133, respectively) are associated with xylan.[58,59] The compounds recorded for $C_3H_5O^+$, $C_4H_5O_2^+$, and $C_5H_5O_2^+$ emerge from detaching H_2O and CO from the quasi-molecular carbohydrate ions.[58] Low-intensity peaks at m/z 107, 121, 151, 167, and 181 suggest the presence of lignin residues, such as guaiacyl and syringyl units, residing in low concentrations in dissolving pulp also end up inside the cellulose beads.[60] The positive ion spectrum, spanning m/z 80.05−155.16, is displayed for cellulose and diamine beads (Figure 3).

Table 1. Characteristic Fragments Present in the Positive and Negative Spectra from the Ionized Samples

material	secondary ion	m/z signal
cellulose	$C_6H_7O_3^+$	127.04
	$C_6H_9O_4^+$	145.05
4,4′-methylenedianiline	$C_7H_8N^+$	106.07
	CN^-	26.00
4,4′-oxydianiline	$C_6H_6NO^+$	108.05
	CN^-	26.00
4,4′-sulfonyldianiline	$C_6H_6NO^+$	108.05
	$C_6H_6NSO^+$	140.02
	CN^-	26.00
	SO_2^-	63.96
diamine cellulose	$C_9H_8N^+$	130.06

The compound CHO is readily released by aldehydes and regular carbohydrates. After normalizing this peak against the peak related to $C_6H_9O_4^+$, the signal for the oxidized beads becomes more prominent than that for cellulose and amino cellulose beads, proving the formation of dialdehyde cellulose. Peaks in the fragmentation patterns of the pure diamines were used to identify the presence of the diamines on the cellulose surface. Fragmentation of pure 4,4′-methylenedianiline gives rise to the formation of $C_7H_8N^+$ with m/z 106. This cationic compound is present in the TOF-SIMS spectrum of C-diamine beads, Figure 3, and indicates the formation of a tropylium derivative. The mass spectrum of ionized 4,4′-oxydianiline and 4,4′-sulfonyldianiline displays a signal at m/z 108. The TOF-SIMS spectrum of the O-diamine beads clearly reveals the presence of 4,4′-oxydianiline on the bead surface, but the intensity of the signal is lower for the S-diamine beads. In S-diamine beads, the signal corresponding to $C_6H_6NSO^+$ at m/z 140 is likewise small. The lower intensity for the S-diamine beads may indicate a lower degree of functionalization than those for the other two samples. In the negative spectrum (not shown), all amine beads reveal a very large peak at CN^-. Also, a clear SO_2^- peak (m/z 64) is found only for the diamine bead containing the sulfone group.

Interestingly, in the positive spectrum for the diamine beads, a peak reveals the presence of compound $C_9H_8N^+$ (m/z 130) on the surface layer, while this signal is absent in the fragmentation pattern of the pure diamines. While rearrangement patterns for diphenyl ethers were elucidated earlier,[61,62] Baira and co-workers further expanded on this earlier work, demonstrating that protonated diphenyl and phenyl pyridyl ethers go through various rearrangements resulting in a multitude of ion compound peaks. This rearrangement process is caused by the interaction between the aromatic rings.[63] Here, after ionization, the molecular fragments from the diamine cellulose possibly go through a similar rearrangement eventually forming $C_9H_8N^+$.

Figure 4 reveals the impact of cellulose oxidation duration and diamine spacer arm selection on the enzymatic activity of the beads. Regardless of the selected spacer arm, 4 h oxidation provided greater enzymatic activity. Two-hour oxidation is likely lacking in surface functionality, thereby binding less protein on the surface. Higher degrees of functionalization, such as the case after 8 h oxidation, may cause excessive enzyme−bead cross-linking, hindering protein dynamics and therefore activity. Unlike 4 h oxidation, for 2 and 8 h oxidation, the spacer arm has minimal influence on reducing sugar production. Xylanase-activated beads display activities of 5.1 ±

https://doi.org/10.1021/acs.biomac.2c00998
Biomacromolecules 2023, 24, 132−140

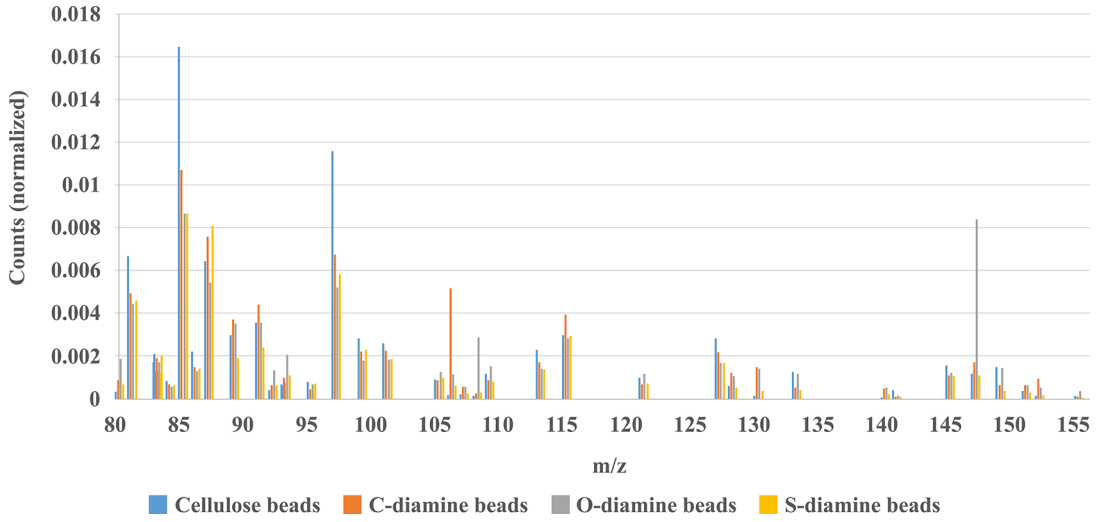

Figure 3. TOF-SIMS spectra in the positive mode for cellulose beads and beads functionalized with 4,4′-methylenedianiline, 4,4′-oxydianiline, and 4,4′-sulfonyldianiline (after 4 h oxidation) with the m/z range spanning from 80 to 155.

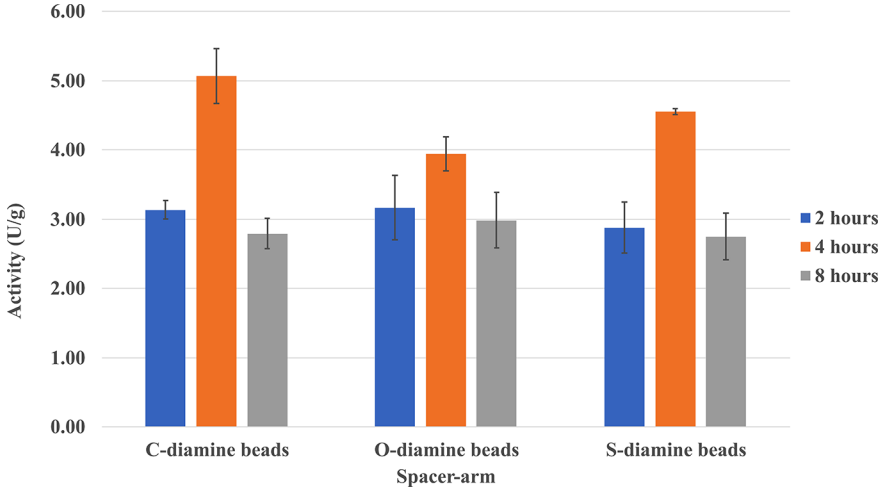

Figure 4. Immobilized endoxylanase activity determined at 80 °C in an acetate buffer pH 5; 2, 4, and 8 h refer to the initial oxidation time. Four-hour periodate oxidation promotes enzymatic activity.

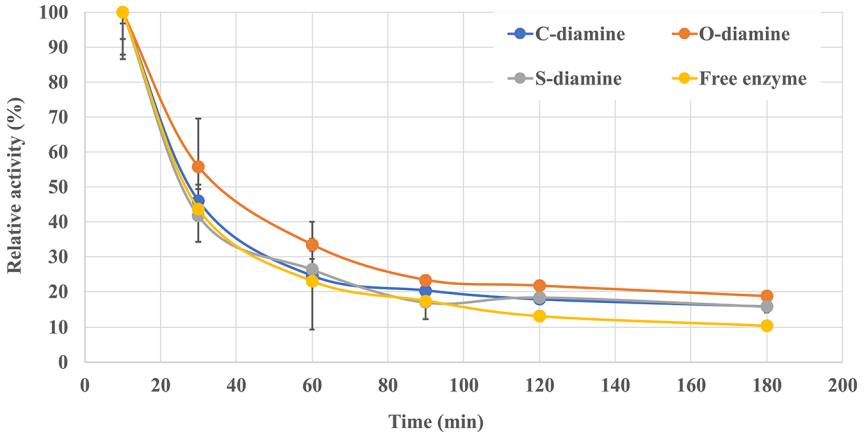

Figure 5. Activity (pH 5, 80 °C) decreases rapidly for both immobilized (beads oxidized for 4 h) and free enzymes. Immobilization enhances the stability of xylanase in particular past the 90 min mark.

0.4, 3.9 ± 0.3, and 4.6 ± 0.1 U/g_{beads} for C-diamine-, O-diamine-, and S-diamine-activated beads when 4 h oxidation was applied. While the immobilization yield is high, 66.7 ± 3.5, 74.5 ± 2.1, and 70.4 ± 0.8% for the respective samples, the immobilized activity is considerably lower with 4.9 ± 0.5, 3.8 ± 0.3, and 4.3 ± 0.1%. The underlying cause for the IA reduction

https://doi.org/10.1021/acs.biomac.2c00998
Biomacromolecules 2023, 24, 132−140

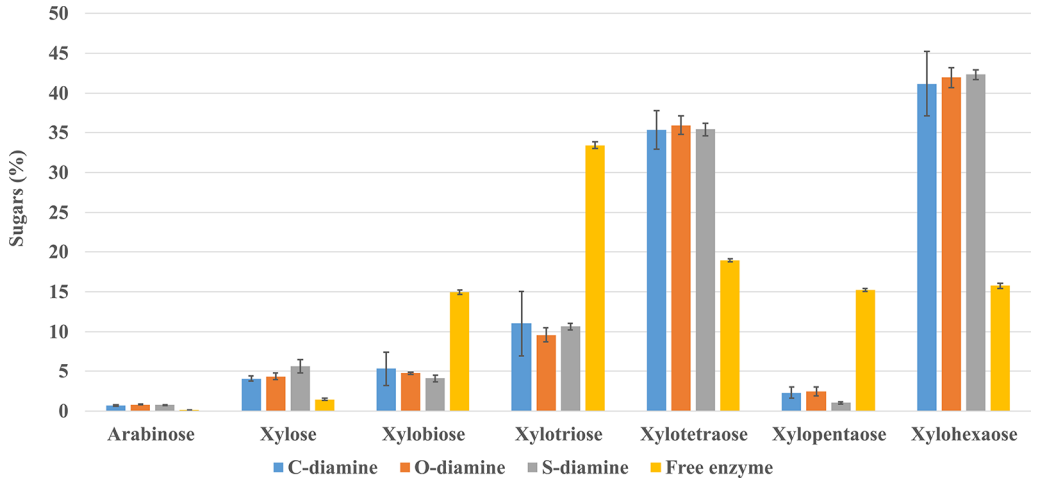

Figure 6. Composition of enzymatically hydrolyzed beechwood xylan after conversion for 24 h at 80 °C, pH 5 with a starting concentration of 1 g/100 mL xylan. XOS mixtures prepared from immobilized endo-1,4-*β*-xylanase (beads initially oxidized for 4 h) were despite delivering a lower XOS yield extensively enriched in xylotetraose and xylohexaose.

is likely due to all of the enzyme activity being concentrated just in one spot, the external sphere surface. As 4 h oxidation proved superior, the diamine beads subjected to 4 h oxidation were studied more in depth.

Compared to porous systems, the obtained activities in this work are lower. Milessi and co-workers reached an activity of 16.3 U/g_{beads} when immobilizing xylanase from *Bacillus subtilis* on porous glyoxal−agarose beads when a similar enzyme load was offered. This value could be further increased by increasing the protein load to 105 U/$g_{beads.}$[52] Similarly, Kapoor and Kuhad also reported greater activities in immobilized xylanase from *Bacillus pumilus* when using enzyme loads of 1000 U/g with birchwood xylan.[23] Others have reported activities up to 62.6 U/g_{beads} using a purolite-based support material again using a higher protein load.[14] The limited available surface, due to the selected drying technique, together with the overall lower enzyme load supplied to the carrier for conjugation explains the lower enzymatic activities obtained for the dense amino cellulose beads. Dense cellulose xerogel beads were chosen as carriers to target the synthesis of XOSs with DPs > 3, as porous systems are known to target the fabrication of xylobiose and xylotriose.[50,52]

The xylanase activity decreases rapidly at 80 °C in both immobilized and free enzyme systems, as indicated in Figure 5. Limited gains in protein stability were achieved after immobilization with no distinct difference between the samples. After 3 h, xylanase immobilized on C-, O-, and S-diamine beads retained 16%, 18%, and 16% of their initial activity, while unbound xylanase retained 10% of its activity under identical conditions. The compositions of xylooligosaccharide mixtures were studied after enzymatic hydrolysis for 24 h, as displayed in Figure 6. Only levels of nonsubstituted xylooligosaccharides were analyzed from the XOS solution. No arabinose was detected in the final XOS mixture. The xylose (X_1) concentration, a side product in XOS production, remained low for the immobilized samples. Its presence is undesired, as it lowers XOS yield and may inhibit xylanase activity.[12] Further, it was observed that XOS mixtures were enriched in xylotetraose (X_4) and xylohexaose (X_6) with surprisingly limited availability in xylopentaose (X_5). Xylanase bound on C-diamine-, O-diamine-, and S-diamine-functionalized beads provided XOS yields of 42.81, 37.91, and 58.27 mg/g, respectively. The functionalization of oxidized cellulose beads with 4,4′-sulfonyldianiline greatly increased the yield over the other spacer arms. The XOS yield obtained using the same quantity of the free enzyme as employed in the immobilization was 392.59 mg/g, in which less than 1% displayed DPs between 4 and 6. To observe which oligosaccharide fractions appear at XOS concentrations similar to those obtained with immobilized xylanase, a slightly more diluted free enzyme solution was used for xylan hydrolysis, resulting in a yield of 26.94 mg/g XOS. These XOS fractions are displayed in Figure 6.

Higher XOS yields in immobilized systems have been demonstrated before, even up to 515 mg/g.[50] However, that study made use of corncob xylan as a substrate source and a porous carrier to achieve this yield. Their XOS formulation mainly consisted of xylobiose (X_2) and xylotriose (X_3) with minor amounts of X_4, while X_5 was absent in the XOS mixture. A similar observation was made by Milessi and co-workers using a porous agarose-glyoxal support in which the retrieved XOS was composed of a combination of X_2−X_4. After 24 h, the mixture contained between 223 and 246 mg/g XOS, depending on the used substrate, with a large fraction of sugars having DPs ≥ 7.[52] Higher-DP XOS production has, to the best of our knowledge, only been demonstrated earlier using nanoparticle carriers as performed by Shivudu and co-workers. Their findings further confirm that the xylan source as well as the carrier material impacts the final XOS compositions. For commercial beechwood xylan, the immobilization on carbon nanoparticles enhanced selectivity for high-DP XOSs, but this lowered the final XOS yield. The use of silica particles was favored in the preparation of high-DP XOSs when handling sugarcane bagasse xylan.[64] The X_2 and X_3 fractions in this work were limited up to 6% and 12%, respectively, but were instead obtained using nonporous beads with a diameter exceeding 1 mm. Thus, while the nonporous functionalized carriers enabled this shift toward higher-DP fractions, it comes at the cost of lower XOS productivity.

With the increasing interest in rational design in enzyme immobilization, the identification and engineering of enzymes received great attention in the last few decades.[16,65] Despite the great interest in the development of new enzyme systems, enzymes are mainly conjugated without engineering the carrier

https://doi.org/10.1021/acs.biomac.2c00998
Biomacromolecules 2023, 24, 132−140

surface. Often, the proteins are conjugated on simple carriers such as activated alginate,[25] agarose,[14,27] or chitosan[27,66] in which the immobilization simply just differs in the mode of conjugation, the cross-linking densities or, alternatively, the performances of completely different supports are compared to one other.

It is generally accepted that the carrier contributes to the microenvironment by enabling the orientation of enzymes during the immobilization, enhancing stability, and impacting activity and selectivity.[16] To introduce small changes in the enzyme microenvironment, beads with three distinct tethers were fabricated. While xylanase conjugation on 4,4′-methylenedianiline-activated beads provides greater activity, over the course of 24 h more XOSs are fabricated exploiting S-diamine beads. The diamines here displayed a highly similar structure, yet by changing the central moiety in the diamine, enzymatic activity was affected. Nevertheless, the XOS fractions remained nearly identical regardless of the chosen spacer arm. This work therefore stresses the need for proper carrier design as an integral part of protein immobilization to exploit the full potential of enzymes. Furthermore, the XOSs fabricated in this work are quite unique for immobilized endo-1,4-β-xylanase, enriched in higher-DP oligosaccharides.

CONCLUSIONS

With the goal of producing xylooligosaccharides with DPs between 4 and 6, we engineered cellulose beads with different spacer arms to study the impact of the spacer arm on enzymatic XOS fabrication. Cellulose beads were initially functionalized with 4,4′-methylenedianiline, 4,4′-oxydianiline, and 4,4′-sulfonyldianiline, and the bead surface was consequently analyzed with TOF-SIMS, confirming the presence of the tethers. Endo-1,4-β-xylanase from *T. maritima* immobilized on 4,4′-methylenedianiline-, 4,4′-oxydianiline-, and 4,4′-sulfonyldianiline-activated beads resulted in activities of 5.06, 3.93, and 4.55 U/g_{beads} with XOS yields of 42.81, 37.91, and 58.27 mg/g, respectively. Approximately 80% of XOSs had DPs between 4 and 6. On the other hand, XOSs fabricated using the free enzyme presented a substantial fraction of xylobiose and xylotriose. In summary, the conjugation altered the selectivity of endo-1,4-β-xylanase toward xylooligosaccharides with higher degrees of polymerization. This work further proved that even minor changes to spacer arms greatly impact the performance of the immobilized xylanase, highlighting the importance of carrier surface engineering in immobilizing xylanase for XOS production.

AUTHOR INFORMATION

Corresponding Author

Pedro Fardim − *Chemical and Biochemical Reactor Engineering and Safety Section, Department of Chemical engineering, KU Leuven, 3001 Leuven, Belgium;* orcid.org/0000-0003-1545-3523; Email: pedro.fardim@kuleuven.be

Authors

Pieter De Wever − *Chemical and Biochemical Reactor Engineering and Safety Section, Department of Chemical engineering, KU Leuven, 3001 Leuven, Belgium*

Charlotte De Schepper − *Laboratory of Food Chemistry and Biochemistry & Leuven Food Science and Nutrition Research Centre (LFoRCe), Department of Microbial and Molecular Systems, KU Leuven, 3001 Leuven, Belgium*

Claude Poleunis − *Institute of Condensed Matter and Nanosciences, UCLouvain, 1348 Louvain-la-Neuve, Belgium*

Arnaud Delcorte − *Institute of Condensed Matter and Nanosciences, UCLouvain, 1348 Louvain-la-Neuve, Belgium;* orcid.org/0000-0003-4127-8650

Christophe M. Courtin − *Laboratory of Food Chemistry and Biochemistry & Leuven Food Science and Nutrition Research Centre (LFoRCe), Department of Microbial and Molecular Systems, KU Leuven, 3001 Leuven, Belgium;* orcid.org/0000-0002-1203-9063

Complete contact information is available at: https://pubs.acs.org/10.1021/acs.biomac.2c00998

Author Contributions

P.D.W. both fabricated and modified cellulose beads and executed the experiments related to immobilization; C.D.S. performed HPAEC-IPAD; C.P. performed TOF-SIMS; P.D.W., P.F., and C.P. contributed to writing; P.F., C.C., and A.D. provided funding to perform the research; and P.D.W., C.C., and P.F. reviewed and edited the manuscript.

Notes

The authors declare no competing financial interest.

ACKNOWLEDGMENTS

Kenneth Simoens from Chemical and Biochemical Reactor Engineering and Safety Section, Department of Chemical engineering, KU Leuven is acknowledged for laboratory support.

ABBREVIATIONS

DP, degree of polymerization; XS, xylooligosaccharides; TOF-SIMS, time of flight secondary ion mass spectroscopy; DMAc, *N*,*N*-dimethylacetamide; DNS, dinitrosalicylic acid; IY, immobilization yield; AY, activity yield; HPAEC-IPAD, high-performance anion exchange chromatography with integrated pulsed amperometric detection; X_1, xylose; X_2, xylobiose; X_3, xylotriose; X_4, xylotetraose; X_5, xylopentaose; X_6, xylohexaose

REFERENCES

(1) Sanders, M. E.; Merenstein, D. J.; Reid, G.; Gibson, G. R.; Rastall, R. A. Probiotics and Prebiotics in Intestinal Health and Disease: From Biology to the Clinic. *Nat. Rev. Gastroenterol. Hepatol.* **2019**, *16*, 605−616.

(2) Everard, A.; Cani, P. D. Diabetes, Obesity and Gut Microbiota. *Best Pract. Res. Clin. Gastroenterol.* **2013**, *27*, 73−83.

(3) Al-Sheraji, S. H.; Ismail, A.; Manap, M. Y.; Mustafa, S.; Yusof, R. M.; Hassan, F. A. Prebiotics as Functional Foods: A Review. *J. Funct. Foods* **2013**, *5*, 1542−1553.

(4) Oniszczuk, A.; Oniszczuk, T.; Gancarz, M.; Szymańska, J. Role of Gut Microbiota, Probiotics and Prebiotics in the Cardiovascular Diseases. *Molecules* **2021**, *26*, 1172.

(5) Dahiya, D. K.; Renuka; Puniya, M.; Shandilya, U. K.; Dhewa, T.; Kumar, N.; Kumar, S.; Puniya, A. K.; Shukla, P. Gut Microbiota Modulation and Its Relationship with Obesity Using Prebiotic Fibers and Probiotics: A Review. *Front. Microbiol.* **2017**, *8*, No. 563.

(6) Butler, M. I.; Mörkl, S.; Sandhu, K. V.; Cryan, J. F.; Dinan, T. G. The Gut Microbiome and Mental Health: What Should We Tell Our Patients?: Le Microbiote Intestinal et La Santé Mentale: Que Devrions-Nous Dire à Nos Patients? *Can. J. Psychiatry* **2019**, *64*, 747−760.

(7) Quigley, E. M. M. Prebiotics and Probiotics in Digestive Health. *Clin. Gastroenterol. Hepatol.* **2019**, *17*, 333−344.

(8) Hills, R.; Pontefract, B.; Mishcon, H.; Black, C.; Sutton, S.; Theberge, C. Gut Microbiome: Profound Implications for Diet and Disease. *Nutrients* **2019**, *11*, 1613.
(9) Broekaert, W. F.; Courtin, C. M.; Verbeke, K.; Van de Wiele, T.; Verstraete, W.; Delcour, J. A. Prebiotic and Other Health-Related Effects of Cereal-Derived Arabinoxylans, Arabinoxylan-Oligosaccharides, and Xylooligosaccharides. *Crit. Rev. Food Sci. Nutr.* **2011**, *51*, 178−194.
(10) Verspreet, J.; Damen, B.; Broekaert, W. F.; Verbeke, K.; Delcour, J. A.; Courtin, C. M. A Critical Look at Prebiotics Within the Dietary Fiber Concept. *Annu. Rev. Food Sci. Technol.* **2016**, *7*, 167−190.
(11) Saad, N.; Delattre, C.; Urdaci, M.; Schmitter, J. M.; Bressollier, P. An Overview of the Last Advances in Probiotic and Prebiotic Field. *LWT–Food Sci. Technol.* **2013**, *50*, 1−16.
(12) Carvalho, A. F. A.; de Oliva Neto, P.; da Silva, D. F.; Pastore, G. M. Xylo-Oligosaccharides from Lignocellulosic Materials: Chemical Structure, Health Benefits and Production by Chemical and Enzymatic Hydrolysis. *Food Res. Int.* **2013**, *51*, 75−85.
(13) Santibáñez, L.; Henríquez, C.; Corro-Tejeda, R.; Bernal, S.; Armijo, B.; Salazar, O. Xylooligosaccharides from Lignocellulosic Biomass: A Comprehensive Review. *Carbohydr. Polym.* **2021**, *251*, No. 117118.
(14) Romero-Fernández, M.; Moreno-Perez, S.; H Orrego, A.; Martins de Oliveira, S.; I Santamaría, R.; Díaz, M.; Guisan, J. M.; Rocha-Martin, J. Designing Continuous Flow Reaction of Xylan Hydrolysis for Xylooligosaccharides Production in Packed-Bed Reactors Using Xylanase Immobilized on Methacrylic Polymer-Based Supports. *Bioresour. Technol.* **2018**, *266*, 249−258.
(15) Aragon, C. C.; Santos, A. F.; Ruiz-Matute, A. I.; Corzo, N.; Guisan, J. M.; Monti, R.; Mateo, C. Continuous Production of Xylooligosaccharides in a Packed Bed Reactor with Immobilized−Stabilized Biocatalysts of Xylanase from Aspergillus Versicolor. *J. Mol. Catal. B: Enzym.* **2013**, *98*, 8−14.
(16) Cao, L.*Carrier-Bound Immobilized Enzymes*; Wiley-VCH Verlag GmbH & Co. KGaA: Weinheim, FRG, 2005.
(17) Liab, K.; Azadi, P.; Collins, R.; Tolan, J.; Kim, J. S.; Eriksson, K. E. L. Relationships between Activities of Xylanases and Xylan Structures. *Enzyme Microb. Technol.* **2000**, *27*, 89−94.
(18) Yagi, H.; Takehara, R.; Tamaki, A.; Teramoto, K.; Tsutsui, S.; Kaneko, S. Functional Characterization of the GH10 and GH11 Xylanases from *Streptomyces olivaceoviridis* E-86 Provide Insights into the Advantage of GH11 Xylanase in Catalyzing Biomass Degradation. *J. Appl. Glycosci.* **2019**, *66*, 29−35.
(19) Fan, G.; Yang, S.; Yan, Q.; Guo, Y.; Li, Y.; Jiang, Z. Characterization of a Highly Thermostable Glycoside Hydrolase Family 10 Xylanase from Malbranchea Cinnamomea. *Int. J. Biol. Macromol.* **2014**, *70*, 482−489.
(20) Çakmakçi, E.; Yuce-Dursun, B.; Demir, S. Maleic Anhydride Functionalization of OSTE Based Coatings via Thiol-Ene "Click" Reaction for the Covalent Immobilization of Xylanase. *React. Funct. Polym.* **2017**, *111*, 38−43.
(21) Romero-Fernández, M.; Moreno-Perez, S.; Martins de Oliveira, S.; Santamaría, R. I.; Guisan, J. M.; Rocha-Martin, J. Preparation of a Robust Immobilized Biocatalyst of β-1,4-Endoxylanase by Surface Coating with Polymers for Production of Xylooligosaccharides from Different Xylan Sources. *New Biotechnol.* **2018**, *44*, 50−58.
(22) Martins de Oliveira, S.; Velasco-Lozano, S.; Orrego, A. H.; Rocha-Martín, J.; Moreno-Pérez, S.; Fraile, J. M.; López-Gallego, F.; Guisán, J. M. Functionalization of Porous Cellulose with Glyoxyl Groups as a Carrier for Enzyme Immobilization and Stabilization. *Biomacromolecules* **2021**, *22*, 927−937.
(23) Kapoor, M.; Kuhad, R. C. Immobilization of Xylanase from Bacillus Pumilus Strain MK001 and Its Application in Production of Xylo-Oligosaccharides. *Appl. Biochem. Biotechnol.* **2007**, *142*, 125−138.
(24) Singh, R. D.; Talekar, S.; Muir, J.; Arora, A. Low Degree of Polymerization Xylooligosaccharides Production from Almond Shell Using Immobilized Nano-Biocatalyst. *Enzyme Microb. Technol.* **2019**, *130*, No. 109368.
(25) Hu, J.; Davies, J.; Mok, Y. K.; Arato, C.; Saddler, J. N. The Potential of Using Immobilized Xylanases to Enhance the Hydrolysis of Soluble, Biomass Derived Xylooligomers. *Materials* **2018**, *11*, 2005.
(26) Shahrestani, H.; Taheri-Kafrani, A.; Soozanipour, A.; Tavakoli, O. Enzymatic Clarification of Fruit Juices Using Xylanase Immobilized on 1,3,5-Triazine-Functionalized Silica-Encapsulated Magnetic Nanoparticles. *Biochem. Eng. J.* **2016**, *109*, 51−58.
(27) Gómez, S.; Payne, A. M.; Savko, M.; Fox, G. C.; Shepard, W. E.; Fernandez, F. J.; Cristina Vega, M. Structural and Functional Characterization of a Highly Stable Endo-β-1,4-Xylanase from Fusarium Oxysporum and Its Development as an Efficient Immobilized Biocatalyst. *Biotechnol. Biofuels* **2016**, *9*, No. 191.
(28) de Oliveira, S. M.; Moreno-Perez, S.; Terrasan, C. R. F.; Romero-Fernández, M.; Vieira, M. F.; Guisan, J. M.; Rocha-Martin, J. Covalent Immobilization-Stabilization of β-1,4-Endoxylanases from Trichoderma Reesei: Production of Xylooligosaccharides. *Process Biochem.* **2018**, *64*, 170−176.
(29) Albuquerque, T. L. d.; Rueda, N.; dos Santos, J. C. S.; Barbosa, O.; Ortiz, C.; Binay, B.; Özdemir, E.; Gonçalves, L. R. B.; Fernandez-Lafuente, R. Easy Stabilization of Interfacially Activated Lipases Using Heterofunctional Divinyl Sulfone Activated-Octyl Agarose Beads. Modulation of the Immobilized Enzymes by Altering Their Nanoenvironment. *Process Biochem.* **2016**, *51*, 865−874.
(30) Rodrigues, R. C.; Virgen-Ortíz, J. J.; dos Santos, J. C. S.; Berenguer-Murcia, Á.; Alcantara, A. R.; Barbosa, O.; Ortiz, C.; Fernandez-Lafuente, R. Immobilization of Lipases on Hydrophobic Supports: Immobilization Mechanism, Advantages, Problems, and Solutions. *Biotechnol. Adv.* **2019**, *37*, 746−770.
(31) Abaházi, E.; Lestál, D.; Boros, Z.; Poppe, L. Tailoring the Spacer Arm for Covalent Immobilization of *Candida antarctica* Lipase B—Thermal Stabilization by Bisepoxide-Activated Aminoalkyl Resins in Continuous-Flow Reactors. *Molecules* **2016**, *21*, 767.
(32) Tiller, J. C.; Rieseler, R.; Berlin, P.; Klemm, D. Stabilization of Activity of Oxidoreductases by Their Immobilization onto Special Functionalized Glass and Novel Aminocellulose Film Using Different Coupling Reagents. *Biomacromolecules* **2002**, *3*, 1021−1029.
(33) Yazgan, I.; Turner, E. G.; Cronmiller, L. E.; Tepe, M.; Ozturk, T. K.; Elibol, M. Modification of Chitosan-Bead Support Materials with l-Lysine and l-Asparagine for α-Amylase Immobilization. *Bioprocess Biosyst. Eng.* **2018**, *41*, 423−434.
(34) Gericke, M.; Trygg, J.; Fardim, P. Functional Cellulose Beads: Preparation, Characterization, and Applications. *Chem. Rev.* **2013**, *113*, 4812−4836.
(35) Trygg, J.; Fardim, P.; Gericke, M.; Mäkilä, E.; Salonen, J. Physicochemical Design of the Morphology and Ultrastructure of Cellulose Beads. *Carbohydr. Polym.* **2013**, *93*, 291−299.
(36) Druel, L.; Niemeyer, P.; Milow, B.; Budtova, T. Rheology of Cellulose-[DBNH][CO 2 Et] Solutions and Shaping into Aerogel Beads. *Green Chem.* **2018**, *20*, 3993−4002.
(37) Li, B.; Pan, Y.; Zhang, Q.; Huang, Z.; Liu, J.; Xiao, H. Porous Cellulose Beads Reconstituted from Ionic Liquid for Adsorption of Heavy Metal Ions from Aqueous Solutions. *Cellulose* **2019**, *26*, 9163−9178.
(38) Heinze, T.; Siebert, M.; Berlin, P.; Koschella, A. Biofunctional Materials Based on Amino Cellulose Derivatives - A Nano-biotechnological Concept. *Macromol. Biosci.* **2016**, *16*, 10−42.
(39) Berlin, P.; Klemm, D.; Tiller, J.; Rieseler, R. A Novel Soluble Aminocellulose Derivative Type: Its Transparent Film-Forming Properties and Its Efficient Coupling with Enzyme Proteins for Biosensors. *Macromol. Chem. Phys.* **2000**, *201*, 2070−2082.
(40) Berlin, P.; Klemm, D.; Jung, A.; Liebegott, H.; Rieseler, R.; Tiller, J. Film-Forming Aminocellulose Derivatives as Enzyme-Compatible Support Matrices for Biosensor Developments. *Cellulose* **2003**, *10*, 343−367.
(41) Sirviö, J. A.; Anttila, A.-K.; Pirttilä, A. M.; Liimatainen, H.; Kilpeläinen, I.; Niinimäki, J.; Hormi, O. Cationic Wood Cellulose

Films with High Strength and Bacterial Anti-Adhesive Properties. *Cellulose* **2014**, *21*, 3573−3583.
(42) Lindh, J.; Ruan, C.; Strømme, M.; Mihranyan, A. Preparation of Porous Cellulose Beads via Introduction of Diamine Spacers. *Langmuir* **2016**, *32*, 5600−5607.
(43) Jin, L.; Li, W.; Xu, Q.; Sun, Q. Amino-Functionalized Nanocrystalline Cellulose as an Adsorbent for Anionic Dyes. *Cellulose* **2015**, *22*, 2443−2456.
(44) Ojala, J.; Sirviö, J. A.; Liimatainen, H. Preparation of Cellulose Nanocrystals from Lignin-Rich Reject Material for Oil Emulsification in an Aqueous Environment. *Cellulose* **2018**, *25*, 293−304.
(45) Sirviö, J. A.; Visanko, M.; Laitinen, O.; Ämmälä, A.; Liimatainen, H. Amino-Modified Cellulose Nanocrystals with Adjustable Hydrophobicity from Combined Regioselective Oxidation and Reductive Amination. *Carbohydr. Polym.* **2016**, *136*, 581−587.
(46) Poletto, P.; Pereira, G. N.; Monteiro, C. R. M.; Pereira, M. A. F.; Bordignon, S. E.; de Oliveira, D. Xylooligosaccharides: Transforming the Lignocellulosic Biomasses into Valuable 5-Carbon Sugar Prebiotics. *Process Biochem.* **2020**, *91*, 352−363.
(47) Valls, C.; Pastor, F. I. J.; Vidal, T.; Roncero, M. B.; Díaz, P.; Martínez, J.; Valenzuela, S. V. Antioxidant Activity of Xylooligosaccharides Produced from Glucuronoxylan by Xyn10A and Xyn30D Xylanases and Eucalyptus Autohydrolysates. *Carbohydr. Polym.* **2018**, *194*, 43−50.
(48) Van Craeyveld, V.; Swennen, K.; Dornez, E.; Van de Wiele, T.; Marzorati, M.; Verstraete, W.; Delaedt, Y.; Onagbesan, O.; Decuypere, E.; Buyse, J.; De Ketelaere, B.; Broekaert, W. F.; Delcour, J. A.; Courtin, C. M. Structurally Different Wheat-Derived Arabinoxylooligosaccharides Have Different Prebiotic and Fermentation Properties in Rats. *J. Nutr.* **2008**, *138*, 2348−2355.
(49) Moniz, P.; Ho, A. L.; Duarte, L. C.; Kolida, S.; Rastall, R. A.; Pereira, H.; Carvalheiro, F. Assessment of the Bifidogenic Effect of Substituted Xylo-Oligosaccharides Obtained from Corn Straw. *Carbohydr. Polym.* **2016**, *136*, 466−473.
(50) Wu, B.; Yu, Q.; Chang, S.; Pedroso, M. M.; Gao, Z.; He, B.; Schenk, G. Expansin Assisted Bio-Affinity Immobilization of Endoxylanase from Bacillus Subtilis onto Corncob Residue: Characterization and Efficient Production of Xylooligosaccharides. *Food Chem.* **2019**, *282*, 101−108.
(51) Rajagopalan, G.; Shanmugavelu, K.; Yang, K.-L. Production of Xylooligosaccharides from Hardwood Xylan by Using Immobilized Endoxylanase of Clostridium Strain BOH3. *RSC Adv.* **2016**, *6*, 81818−81825.
(52) Milessi, T. S. S.; Kopp, W.; Rojas, M. J.; Manrich, A.; Baptista-Neto, A.; Tardioli, P. W.; Giordano, R. C.; Fernandez-Lafuente, R.; Guisan, J. M.; Giordano, R. L. C. Immobilization and Stabilization of an Endoxylanase from Bacillus Subtilis (XynA) for Xylooligosaccharides (XOs) Production. *Catal. Today* **2016**, *259*, 130−139.
(53) Münster, L.; Vícha, J.; Klofáč, J.; Masař, M.; Kucharczyk, P.; Kuřitka, I. Stability and Aging of Solubilized Dialdehyde Cellulose. *Cellulose* **2017**, *24*, 2753−2766.
(54) Dang, X.; Liu, P.; Yang, M.; Deng, H.; Shan, Z.; Zhen, W. Production and Characterization of Dialdehyde Cellulose through Green and Sustainable Approach. *Cellulose* **2019**, *26*, 9503−9515.
(55) Miller, G. L. Use of Dinitrosalicylic Acid Reagent for Determination of Reducing Sugar. *Anal. Chem.* **1959**, *31*, 426−428.
(56) Fernandes Diniz, J. M. B.; Gil, M. H.; Castro, J. A. A. M. Hornification - Its Origin and Interpretation in Wood Pulps. *Wood Sci. Technol.* **2004**, *37*, 489−494.
(57) Siller, M.; Amer, H.; Bacher, M.; Roggenstein, W.; Rosenau, T.; Potthast, A. Effects of Periodate Oxidation on Cellulose Polymorphs. *Cellulose* **2015**, *22*, 2245−2261.
(58) Fardim, P.; Durán, N. Modification of Fibre Surfaces during Pulping and Refining as Analysed by SEM, XPS and ToF-SIMS. *Colloids Surf., A* **2003**, *223*, 263−276.
(59) Finšgar, M.; Ristić, T.; Fardim, P.; Zemljič, L. F. Time-of-Flight Secondary Ion Mass Spectrometry Analysis of Chitosan-Treated Viscose Fibres. *Anal. Biochem.* **2018**, *557*, 131−141.
(60) Saito, K.; Watanabe, Y.; Shirakawa, M.; Matsushita, Y.; Imai, T.; Koike, T.; Sano, Y.; Funada, R.; Fukazawa, K.; Fukushima, K. Direct Mapping of Morphological Distribution of Syringyl and Guaiacyl Lignin in the Xylem of Maple by Time-of-Flight Secondary Ion Mass Spectrometry. *Plant J.* **2012**, *69*, 542−552.
(61) Guerra, M.; Cabral, M. H.; Paiva, A. C. S. Fragmentation Pathways of Diphenyl Ether Radical Cations. *Int. J. Mass Spectrom.* **2015**, *393*, 9−16.
(62) Ballantine, J. A.; Pillinger, C. T. A Study of Rearrangement Processes in the Mass Spectra of Substituted Diphenyl-Ethers. *Org. Mass Spectrom.* **1968**, *1*, 447−458.
(63) Baira, S. M.; Ragampeta, S.; Talluri, M. V. N. K. A Comprehensive Study on Rearrangement Reactions in Collision-induced Dissociation Mass Spectrometric Fragmentation of Protonated Diphenyl and Phenyl Pyridyl Ethers. *Rapid Commun. Mass Spectrom.* **2019**, *33*, 1440−1448.
(64) Shivudu, G.; Chandraraj, K.; Selvam, P. Production of Xylooligosaccharides from Xylan Catalyzed by Endo-1,4-β-D-Xylanase-Immobilized Nanoscale Carbon, Silica and Zirconia Matrices. *Mol. Catal.* **2020**, *484*, No. 110745.
(65) Ali, M.; Ishqi, H. M.; Husain, Q. Enzyme Engineering: Reshaping the Biocatalytic Functions. *Biotechnol. Bioeng.* **2020**, *117*, 1877−1894.
(66) Guerfali, M.; Maalej, I.; Gargouri, A.; Belghith, H. Catalytic Properties of the Immobilized Talaromyces Thermophilus β-Xylosidase and Its Use for Xylose and Xylooligosaccharides Production. *J. Mol. Catal. B: Enzym.* **2009**, *57*, 242−249.

Recommended by ACS

Preparation of Cellulose Nanofibers from Corn Stalks by Fenton Reaction: A New Insight into the Mechanism by an Experimental and Theoretical Study
Rui-Cheng Qin, Chun-Guang Liu, *et al.*
JANUARY 18, 2023
JOURNAL OF AGRICULTURAL AND FOOD CHEMISTRY
READ

Efficient Conversion of Cellulose to Thermoplastics by Mechanochemical Esterification
De-Fa Hou, Ming-Bo Yang, *et al.*
MAY 10, 2023
ACS SUSTAINABLE CHEMISTRY & ENGINEERING
READ

Top-Down Production of Sustainable and Scalable Hemicellulose Nanocrystals
Xiang Hao, Feng Peng, *et al.*
NOVEMBER 02, 2022
BIOMACROMOLECULES
READ

Unraveling the Supramolecular Structure and Nanoscale Dislocations of Bacterial Cellulose Ribbons Using Correlative Super-Resolution Light and Electron Microscopy
Mouhanad Babi, Jose M. Moran-Mirabal, *et al.*
DECEMBER 28, 2022
BIOMACROMOLECULES
READ

Get More Suggestions >

https://doi.org/10.1021/acs.biomac.2c00998
Biomacromolecules 2023, 24, 132−140